AGU PUBLICATIONS

JGR

Journal of Geophysical Research: Space Physics

RESEARCH ARTICLE
10.1002/2014JA019914

Key Points:
- Latitudinal dependences for Saturn chorus intensity, wave angle, and bandwidth
- Magnetic inhomogeneity at Saturn is much lower than at Earth
- Chorus bandwidth peaks at region of nonlinear growth

Correspondence to:
J. D. Menietti,
john-menietti@uiowa.edu

Citation:
Menietti, J. D., G. B. Hospodarsky, Y. Y. Shprits, and D. A. Gurnett (2014), Saturn chorus latitudinal variations, *J. Geophys. Res. Space Physics*, *119*, 4656–4667, doi:10.1002/2014JA019914.

Received 21 FEB 2014
Accepted 30 MAY 2014
Accepted article online 4 JUN 2014
Published online 24 JUN 2014

Saturn chorus latitudinal variations

J. D. Menietti[1], G. B. Hospodarsky[1], Y. Y. Shprits[2,3,4], and D. A. Gurnett[1]

[1]Department of Physics and Astronomy, University of Iowa, Iowa City, Iowa, USA, [2]Department of Earth and Space Sciences, University of California, Los Angeles, California, USA, [3]Department of Earth Atmospheric and Planetary Sciences, MIT, Cambridge, Massachusetts, USA, [4]Skolkovo Institute of Science and Technology, Moscow, Russia

Abstract The variation of propagation properties of whistler mode chorus as a function of latitude is not well known at Saturn but is important for the calculation of pitch angle diffusion and nonlinear growth of chorus. The Cassini spacecraft has spent a portion of its orbital time in high-inclination orbits, allowing traversal of the magnetic equator at nearly constant L shell for several passes. This is important since chorus is believed to propagate dominantly close to the magnetic field direction. We have investigated the change of wave normal angle, whistler mode magnetic intensity, and ambient magnetic field inhomogeneity as a function of latitude observed by the Radio and Plasma Wave investigation onboard the Cassini instrument. We find that wave normal angles along a nearly constant L shell remain close to field-aligned, except nearest the equator, and whistler mode wave intensity increases from the magnetic equator, according to a power law. The ambient magnetic field shows an inhomogeneity that is lower than Earth's, but there is a lack of drifting-frequency signatures nearest the equator. The bandwidth of the chorus emission can be described by a simple exponential. The bandwidth increases from the equator, peaking a few degrees away in a region of strong nonlinear growth and then decreases at higher latitudes.

1. Introduction

The role of whistler mode chorus emission in accelerating and scattering electrons in the Earth's outer radiation belt is better understood, based on a long history and many recent advances. Chorus emission at the outer planets is also growing in attention. *Horne et al.* [2008] performed Fokker-Planck simulations indicating the effectiveness of pitch angle diffusion to accelerate electrons in the Jovian magnetosphere (between 6 and 12 Jovian radii) to MeV energies within 30 days. *Woodfield et al.* [2013] have more recently extended these studies, incorporating larger chorus bandwidth and extent in L shell of chorus intensity, based on observations, which produces improved effectiveness of chorus electron acceleration to $L > 10$. Because of the importance of a relatively low ratio of plasma frequency to cyclotron frequency, f_p/f_c, for effective pitch angle scattering by chorus waves [*Horne et al.*, 2003], the most efficient wave-particle interactions occur in the outer plasma torus.

The Cassini mission to Saturn has provided the opportunity to gather a large data set of chorus emission as previously summarized by *Hospodarsky et al.* [2008]. Comparison studies of chorus at Jupiter and Saturn [*Hospodarsky et al.*, 2012; *Menietti et al.*, 2012] indicate that Saturn chorus emissions can be intense even at high latitude up to ~30°. However, plasma density measurements generally indicate higher ratios, f_p/f_c, and probably less efficient electron acceleration by chorus [cf. *Shprits et al.*, 2012]. *Mauk and Fox* [2010] suggest that at Saturn, interactions with dust particles may provide an efficient loss of electrons and result in the electron fluxes lower than the Kennel and Petschek limit. Subsequent studies by *Summers et al.* [2012] include relativistic effects in the nonlinear equations, and *Tang and Summers* [2012] have performed a comprehensive study of energetic electron fluxes at Saturn and found that at intermediate L shells, $5 < L < 7$ (where chorus is observed), measured electron fluxes are close to the Kennel-Petschek limit. This is a good indication of whistler mode wave generation that limits trapped electron fluxes.

At Earth the significant source region of chorus emission is known to be near the magnetic equator, but the chorus intensity increases away from this region as reported by *Santolík et al.* [2009] from Cluster observations. The exponential spatial growth of chorus has been reported by *Haque et al.* [2012] from a study of a dozen Cluster orbits. Because the spatial scales at Saturn are much larger, the observation of increasing chorus intensity and bandwidth away from the magnetic equator is more easily detectable [*Menietti et al.,* 2012, 2013a, 2013b]. Accurate modeling of the auroral electron energies by diffusive models requires parameterization of chorus magnetic wave amplitude, frequency distribution, and wave normal angle as a function of latitude,

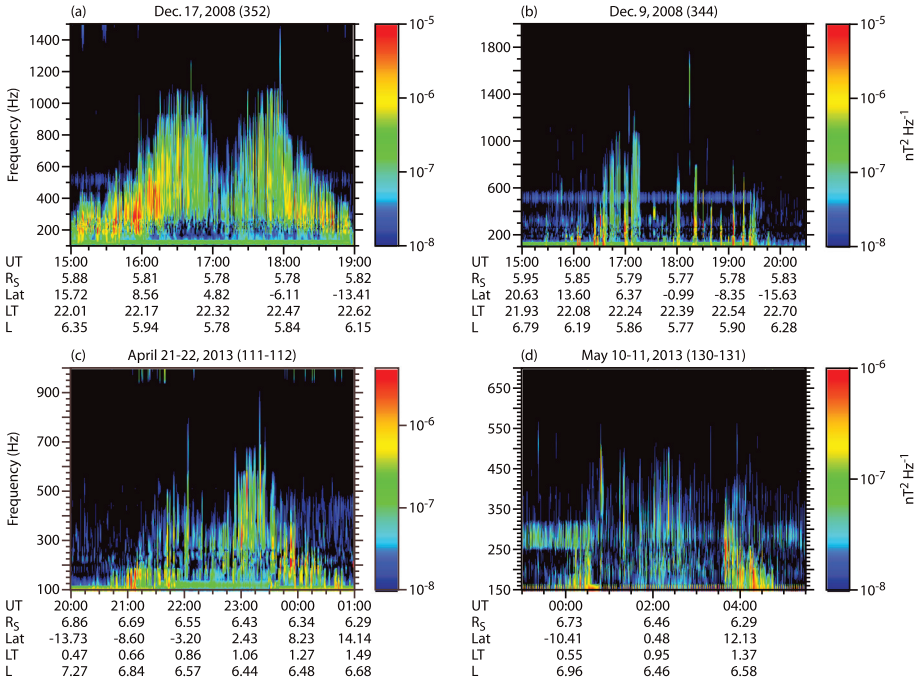

Figure 1. Spectrograms of magnetic wave spectral density versus time are shown in Figure 1 for time intervals on each of these days. (a) Data from 2008/352 and (b) 2008/344 which is an orbit quite similar to Figure 1a, but the chorus intensity is much more bursty. (c) 2013, days 111–112 and (d) 2013, days 130–131.

L, and magnetic local time. Such parameterization of spatial and spectral wave properties has been reported for Earth studies by a number of authors [cf. *Shprits et al.*, 2007; *Li et al.*, 2007; *Shprits and Ni*, 2009; *Spasojevic and Shprits*, 2013]. More recently, multisatellite data have been used to develop parametric models of chorus parameters using data from Van Allen Probes and Polar Orbiting Environment Satellites [cf. *Li et al.*, 2013]. Since relativistic electrons can resonate with field-aligned waves only at high latitudes, the high-latitude chorus is responsible for scattering electrons into the atmosphere [e.g., *Thorne et al.*, 2005]. The latitudinal distribution of waves can change the balance between acceleration and loss and is crucial in determining the pitch angle distribution and energy spectrum of electrons [*Shprits et al.,* 2006]. Such studies are important for global modeling, but no such detailed work has yet been reported for the outer planets. In the present study, we examine examples of whistler mode emission close to the magnetic equator along approximately constant L shell and study the change of wave normal angle, wave intensity, and ambient magnetic field as a function of latitude.

2. Observations

The Cassini spacecraft has made a number of high-inclination orbits beginning in mid-2005, late 2006 to mid-2007, 2008 to mid-2009, and again in 2013. During these orbits, only a few equator crossings have occurred at approximately a constant L shell for latitudes within 10 to 15° of the equator while intercepting the region of intense chorus emission. We single out these few passes to study the observed latitudinal variation of chorus power, wave normal angle, and the ambient magnetic field inhomogeneity. We have chosen data from days 352 and 344 of 2008 and from days 111 and 130 of 2013, for special study, because of the near-constant L shell near the magnetic equator.

Spectrograms of magnetic wave spectral density versus time are shown in Figure 1 for time intervals on each of these days. These data are obtained from the low- (1–26 Hz), medium- (24 Hz–12 kHz), and high- (3.5 kHz–16 MHz) frequency receivers of the Radio and Plasma Wave investigation (RPWS) onboard the Cassini spacecraft [*Gurnett et al.*, 2004]. These receivers can be connected to the electric antennas or the magnetic search coils. However, the magnetic frequency range is limited to about 12 kHz and low-frequency emissions are suppressed due to significant noise in these channels. A characteristic signature of these passes is an enhancement of chorus intensity a few degrees on either side of the magnetic equator, with an intensity

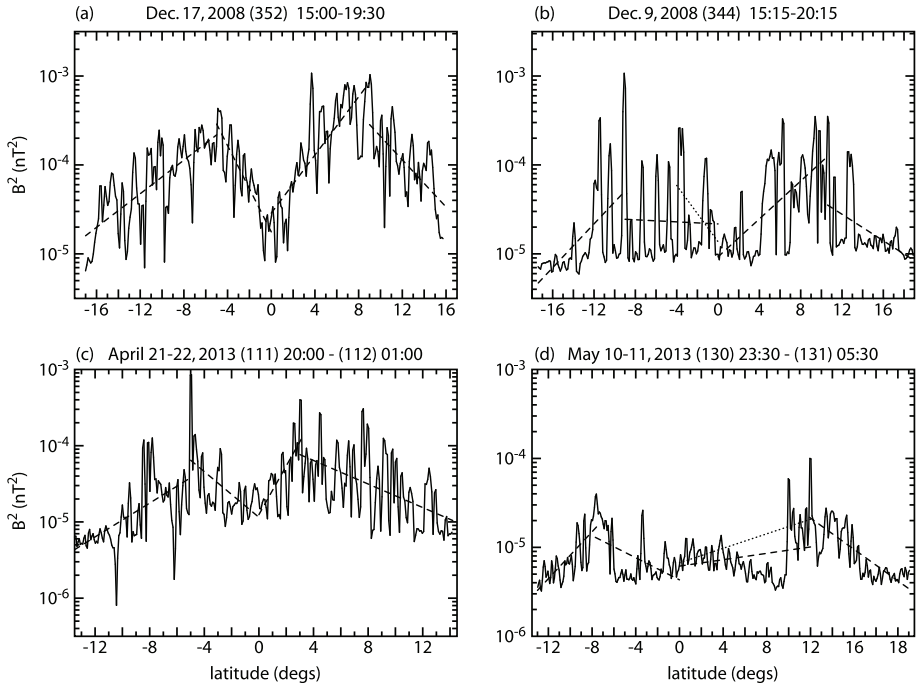

Figure 2. The square of the wave magnetic field intensity versus latitude for each of the passes shown in Figure 1. Each panel displays the calculated value of wave magnetic field, B^2, proportional to power, over the approximate frequency range of 200 Hz to the extent of the chorus frequency (~2 kHz) for each pass. A linear least squares fit to the data is overplotted with a dashed line. (a) 17 December 2008 (352). (b) The dotted line is the fit which does not include the data between $-9° < \lambda < -4°$, where a number of plasma injections are encountered. (c) 21–22 April 2013 (111)–(112). (d) We include a dotted line slope which omits the data in the range $0° < \lambda < 10°$.

minimum nearest the magnetic equator. For unknown reasons the overall power appears somewhat greater in the northern hemisphere on each pass. For the passes in Figures 1a and 1b, the spacecraft orbit is nearly symmetric in L across the equator, but in Figures 1c and 1d there is somewhat of an asymmetry across the equator. This is due to the smaller inclination of the orbit during the passes of 2013 compared to 2008.

Data from 2008/352, Figure 1a, have been published in the past [cf. *Menietti et al.,* 2012, 2013a, 2013b]. This orbit shows rather intense chorus emissions near the equator for a near-constant $L \sim 5.8$ within ~±10° of the equator. Figure 1b is for 2008/344, which is an orbit quite similar to Figure 1a, but here the chorus intensity is much more bursty. This is due in part to the large number of plasma injection regions encountered during this time period. Figures 1c and 1d for 2013 on days 111–112 and 130–131 have modest chorus intensity, but the orbit inclination is smaller and, as mentioned, while crossing the magnetic equator, the L shell varies more than for Figures 1a and 1b. In Figure 1c we see a pattern similar to Figure 1a, but the satellite is on a higher L shell ($L \sim 6.5$) and the spacecraft radius decreases during the crossing of the equator. Finally, Figure 1d is similar to Figure 1c but misses the region of most intense chorus because of the evolving orbit with slowly varying radius and longitude.

2.1. Power Versus Latitude

In Figure 2, we display the square of the wave magnetic field intensity versus latitude, λ, for each of the passes shown in Figure 1. Each panel displays the calculated value of wave magnetic field, B^2, proportional to magnetic power, over the approximate frequency range of 200 Hz to ~2 kHz, the extent of the chorus frequency for each pass. Knowledge of the magnetic wave power is directly useful for modeling chorus wave-particle interactions that may scatter or accelerate electrons. The plots indicate regions of increasing power away from the equator (spatial growth) reaching a peak, then decreasing with latitude away from the equator. For the data of Figures 2a and 2c, the regions are relatively easy to discern, but more care is needed for data of Figures 2b and 2d. The divisions shown in each panel of Figure 2 were made by eye, judging the point where there appears to be a general change in slope. Least squares fits are made to the regions of growth and decay (dashed curves), and special dotted curves are also included in Figures 2b and 2d. In

Table 1. Chorus Spatial Growth, γ_s (Degrees^{-1})

Orbit Year/Day	Southern Hemisphere	Northern Hemisphere
2008/352	−0.28	0.19
2008/344	−.0067 (−0.16)	0.123
2013/111	−0.17	0.37
2013/130	−0.07	0.03 (.047)

Figure 2b, the dotted line denotes the fit which does not include the data between $-9° < \lambda < -4°$, where a number of plasma injections are encountered. This value is in parentheses in Table 1, row 2. In Figure 2d, we include a dotted line slope which omits the data in the range $0° < \lambda < 10°$. In this part of the orbit, the spacecraft radial distance is decreasing, and the L shell begins to increase before encountering the region of intense chorus near $\lambda = 10°$. The change of local time is greater near the equator for this pass than on the other passes, which may explain the small increase in power between 01:30 and 03:00. The slope of the dotted line is recorded in parentheses in row 4. For each panel of Figure 2, the slope of the lines adjacent to the equator in both hemispheres is used to calculate the spatial growth rate according to the expression $P = P_o e^{(2\gamma_s \lambda)}$, where P is the relative power relative to the minimum near the equator and λ is the latitude in degrees. We note that temporal effects are not accounted for in this calculation. We record the measured γ_s (degrees^{-1}) in Table 1. The region of chorus growth shown in the panels of Figure 2 varies in size from ~4° to ~12° of latitude near $L \sim 6$ at Saturn. Interestingly, *Santolik* [2008, and references therein] notes that Cluster observations of chorus at Earth suggest a chorus source region of extent 3000–5000 km near L ~4, corresponding to a range of 6.8° to 11.3° in latitude, not unlike the results for Saturn.

2.2. Wave Normal Angle Versus Latitude

The waveform receiver (WFR) onboard the Cassini spacecraft is five-channel, E_x, E_y (or E_z), and B_x, B_y, and B_z [*Gurnett et al.*, 2004]. The frequency range for this study is 3 Hz to 2.5 kHz. This receiver operates in a snapshot mode typically once each 5 min and provides three-axis magnetic field waveforms for analysis of whistler mode and low-frequency Z mode. We use the Means method [cf. *Means*, 1972; *LeDocq et al.*, 1998] to analyze the spectral waveforms for $f < 2.5$ kHz. In Figure 3, we display an analysis spectrogram of the five-channel waveform receiver data showing the electric and magnetic fields as well as the wave normal directions for chorus emissions for each of the passes of Figure 1. The rows contain (top to bottom) wave electric field, wave magnetic field, wave normal angle (relative to the ambient magnetic field) (θ), azimuthal wave angle (φ), Poynting flux angle (θ_s), and the wave direction (red (green), $\mathbf{S}\cdot\mathbf{B} > 0$ ($\mathbf{S}\cdot\mathbf{B} < 0$)). To calculate Poynting flux with only five channels (three magnetic but only two components of $\mathbf{E}$), the assumption $\mathbf{E}\cdot\mathbf{B} = 0$ is used. Only waves with minimum signal-to-noise ratio and coherence are processed with the wave normal angle (WNA) software tool. Eigenvalues of the spectral matrix are found, and the ratio of the largest eigenvalue to the sum of the eigenvalues is calculated. A ratio of 1 indicates a single, plane wave. Coherency is determined from the cross-spectral index and a determination of the unit wave normal vector. For a wave with the wave normal along the z axis, $C_{xy} = |J_{xy}| / (J_{xx}\, J_{yy})^{1/2}$, where J is the spectral matrix. A value close to 1 indicates a coherent wave. The minimum levels for the data tests are labeled beneath row 1 of Figures 3a–3d.

The plots of Figure 3 provide an overview of the wave directions versus time. In Figure 3a, we present the analysis of day 2008/352 (Figure 1a). The chorus wave normal angles are generally field aligned (within ~30°), directed away from the equator except nearest the equator where mixed directions are observed (bottom two rows), as reported by *Hospodarsky et al.* [2008]. In the spacecraft-centered, field-aligned coordinate system, the z axis is parallel to the ambient magnetic field. The x axis is chosen such that the radial vector from the center of Saturn to the spacecraft is contained in the x-z plane. The y axis completes the right-handed system and points westward. The azimuthal angle φ is measured counterclockwise from the x axis in the x-y plane, so that $\varphi = 0$ points radially outward, while $\varphi = 90$ points westward. In Figure 3b, for day 2008/344 (Figure 1b), the chorus emission is much more bursty, but when present, the wave normal angles also appear to be generally field aligned, within 30° and directed away from the equator. The chorus observed centered near 18:15 at frequencies greater than 700 Hz (indicated by an arrow in rows 3–6) is associated with a plasma injection region. Chorus in plasma injection regions has been studied in the past [cf. *Menietti et al.*, 2008, 2012], where enhancement of the intensity levels was noted, consistent with the warm plasma distributions observed within these regions. However, more studies of these regions are warranted. Larger than normal plasma injections may imply a global change of plasma distributions that are the source of chorus. Figure 3c for day 2013/111 (Figure 1c) indicates a data gap in the region near the equator, where some of the most intense chorus occurs. The remaining times indicate a large

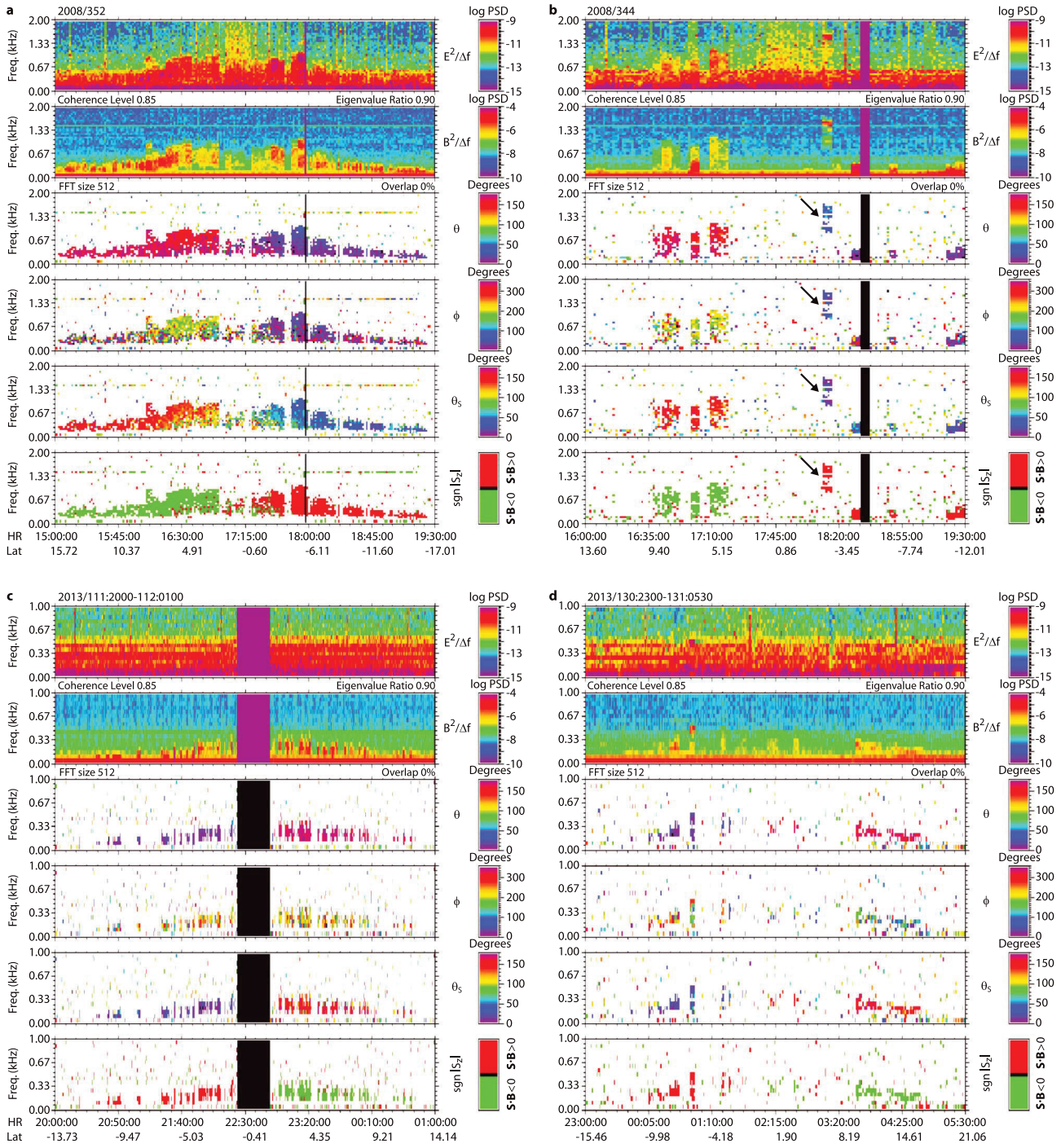

Figure 3. Analysis spectrogram of the five-channel waveform receiver data showing the electric and magnetic fields as well as the wave normal directions for chorus emissions for each of the passes of Figure 1. The rows contain (top to bottom) wave electric field ($V^2\ m^{-2}\ Hz^{-1}$), wave magnetic field ($nT^2\ Hz^{-1}$), wave normal angle (relative to B) (θ), azimuthal wave angle (φ), Poynting flux angle (θ_s), and the wave direction (red (green), $\mathbf{S}\cdot\mathbf{B} > 0$ ($\mathbf{S}\cdot\mathbf{B} < 0$)).

sample of field-aligned wave normal angles, away from the equator, within perhaps 20° to 30°. Finally, Figure 3d for day 2013/130 indicates a significant sampling of field-aligned chorus also within about 30° directed away from the equator. We now look in more detail at the wave normal angles sorted relative to latitude.

In Figure 4a, we present a plot of wave normal angle, θ, versus latitude for the orbit of 2008/352. The coherency and eigenvalue criteria are the same as for Figure 3. We have binned the data into frequency

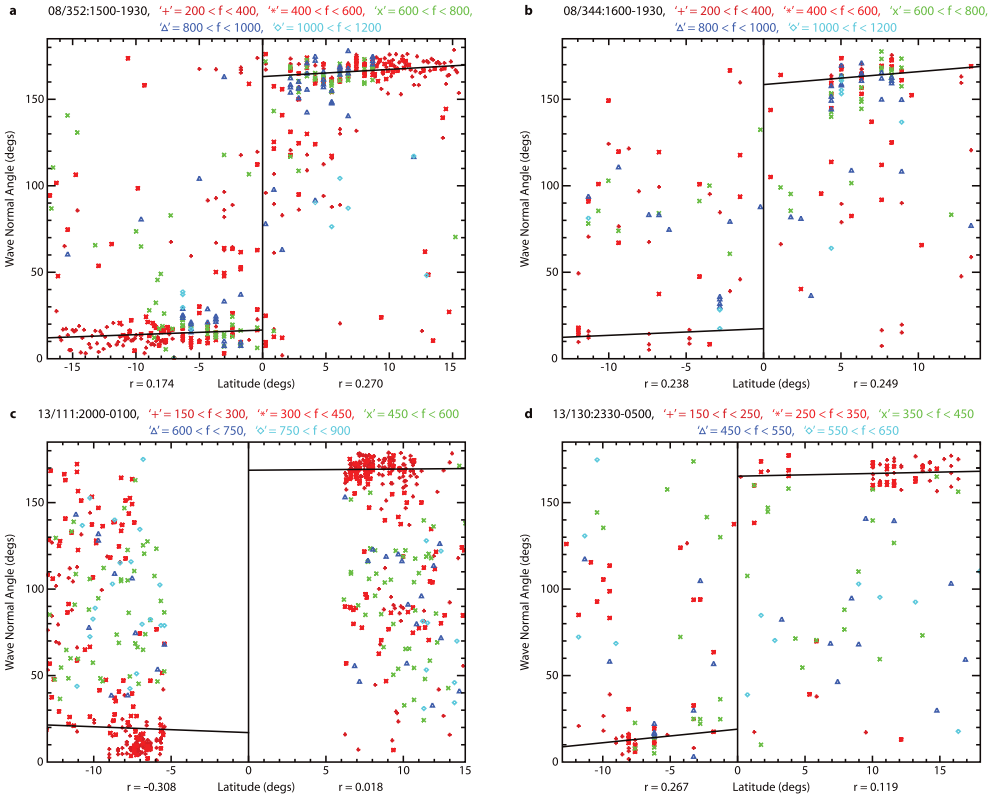

Figure 4. (a) 08/352:1500–1930, (b) 08/344:1600–1930, (c) 13/111:2000–0100, and (d) 13/130:2330–0500. Wave normal angle, θ, versus latitude for each of the passes of Figure 3. The data are limited to power levels $> 10^{-8}$ nT^2 to clarify the plot. We have performed a least squares fit to the data for $\theta < 30°$ (southern hemisphere) and for $\theta > 150°$ (northern hemisphere) which are plotted as lines. The correlation coefficient, *r*, for each line is shown at the bottom of each panel.

ranges: 200 Hz $< f <$ 400 Hz, 400 $< f <$ 600 Hz, 600 $< f <$ 800 Hz, 800 $< f <$ 1000 Hz, and 1000 $< f <$ 1200 Hz. We note that there is a large amount of interference for $f <$ 200 Hz, which is true for each of the data sets to be considered. Most of the chorus emission occurs for $f <$ 1000 Hz, while the most intense observations of frequency-drifting chorus are observed for $f >$ 500 Hz. We have also limited the data to power levels $>10^{-8}$ nT^2 to clarify the plot. The values of θ show a general decrease in scatter with λ. We have performed a least squares fit to the data for $\theta < 30°$ (southern hemisphere) and for $\theta > 150°$ (northern hemisphere), which are plotted as lines. The correlation coefficient, *r*, for the fitted lines in each hemisphere is shown at the bottom of each panel of Figure 4.

In Figure 4b, we plot wave normal angle versus latitude for the pass of 2008/344, one orbit before the data for day 2008/352. The frequency bins for sorting the wave normal angles are the same as in Figure 4a. During the time of this observation, the RPWS observed an unusually high rate of plasma injections [*Hill et al.*, 2005; *Menietti et al.*, 2008]. These injections, which at this time were encountered for periods of a few minutes to tens of minutes, may have contributed to the low rate and bursty nature of chorus emissions for unclear reasons. We mentioned above a possible global change of the plasma distribution during this time. Consequently, we see in Figure 4b more scatter in the value of θ versus latitude. There is a concentration of $\theta > 150°$ for latitudes greater than 4° and a small increase for $\theta < 20°$ for latitude $< -4°$, but the numbers are much less than those observed in Figure 4a, which contained only a few examples of plasma injection regions. We have again included a least squares fit to the data for $\theta < 30°$ (southern hemisphere) and for $\theta > 150°$ (northern hemisphere).

Referring again to the wave spectrogram for 2013 day 111/20:00 to day 112/01:00 (Figure 1c), the spacecraft intercepts the equator near 22:30 and $L \sim 6.5$, where chorus is typically observed. For this particular pass, the chorus intensities and bandwidth are modest, and each is a minimum nearest the equator at ~22:30. As noted above, there is a large region close to the equator where no WFR data were available due to an

instrument mode change. In Figure 4c, we display θ versus λ sorted for this pass over frequency ranges 150 Hz $< f <$ 300 Hz, 300 Hz $< f <$ 450 Hz, 450 Hz $< f <$ 600 Hz, 600 Hz $< f <$ 750 Hz, 750 Hz $< f <$ 900 Hz, and 900 Hz $< f <$ 1050 Hz. The new frequency bins reflect the lower bandwidth of the chorus for this time period. Similar to Figure 4a, we see a concentration of values at $f <$ 500 Hz for $\theta < 20°$ in the south and $\theta > 150°$ in the north, for the approximate range of latitudes $-9° < \lambda < -5°$ and $6° < \lambda < 11°$. The values of θ are well distributed with no particular concentration outside of those near field alignment encountered along the L shell of the chorus source region. Because of a lack of WFR data nearest the equator, the least squares fit to the more field-aligned values of θ actually shows a negative slope for the southern hemisphere.

In Figure 4d, we plot the wave normal angles versus latitude for the case of Figure 1d. The frequency bins for this case are 150 Hz $< f <$ 250 Hz, 250 Hz $< f <$ 350 Hz, 350 Hz $< f <$ 450 Hz, 450 Hz $< f <$ 550 Hz, 550 Hz $< f <$ 650 Hz, and 650 Hz $< f <$ 750 Hz. We see a small concentration of values near field alignment, when the spacecraft encounters the L shell of the chorus source region for latitudes in the approximate range $-10° < \lambda < -5°$ and $\lambda > 9°$ but much scatter at other latitudes. Fits to θ close to the field-aligned direction again yield positive slopes or decreasing wave normal angles away from the equator.

2.3. Magnetic Field Inhomogeneity

Katoh and Omura [2013] discuss the role of background magnetic field inhomogeneity on the nonlinear generation of whistler mode chorus and hiss-like emissions. Following *Omura et al.* [2009] and *Katoh and Omura* [2013] we assume a quadratic variation of the magnetic field close to the magnetic equator. The inhomogeneity is defined relative to a magnetic dipole as

$$\Omega = \Omega_o\left(1 + ah^2\right) \tag{1}$$

where Ω is the electron cyclotron frequency, h is the distance along the magnetic field line from the equator and

$$a = F_a \times 4.5/(LR_s)^2 \tag{2}$$

for the L value and the Saturn radius, R_s, with F_a describing the inhomogeneity from that of a dipole field. For a quadratic approximation of a dipole field, $F_a = 1$. As *Katoh and Omura* [2013] point out, a large inhomogeneity, F_a, yields a large amplitude threshold for nonlinear (frequency-drifting) chorus, while a small value yields a small amplitude threshold for growth of nonlinear broadband ("hiss-like") chorus in self-consistent electron hybrid code simulations. The hiss-like emission discussed by *Katoh and Omura* [2013] is intense nonlinear chorus with rising tones but so saturated that it appears diffuse on simulated spectrograms such as the authors' Figure 3a. Since the Saturn observations indicate more diffuse (hiss-like) emission near the magnetic equator, this may imply a low or dipole-like background magnetic field near the equator.

Rising chorus tones or drifting frequencies are a signature of nonlinear chorus generation as elucidated in *Trakhtengerts et al.* [2004] and *Omura et al.* [2007, 2008]. These tones are generated by resonant currents resulting from the process of wave potential trapping of electrons. An electron hole in the wave phase space [cf. *Omura et al.*, 2008, Figure 1] will form with the depth of the hole, Q, related to the resonant current. If the ambient magnetic field changes rapidly with distance away from the magnetic equator (strong inhomogeneity, as at Earth), then large resonant currents are required. However, Saturn is a massive planet, with an apparent much smaller inhomogeneity, and thus a much smaller resonant current would be required, and the threshold for nonlinear resonance at Saturn should be much lower than at Earth. *Katoh and Omura* [2013] have shown this to be the case in simulations of whistler mode chorus as a function of variable background magnetic field inhomogeneity at Earth. Their results show that smaller inhomogeneities produce a lower threshold (nonlinear triggering process) for rising frequency signatures to emerge, producing a hiss-like (nonlinear diffuse wave) signature on simulated spectrograms.

The orbit of 2008/352 is nearly at constant L shell within about ±8° of the equator. We therefore single out this pass for an examination of the background inhomogeneity as defined in equations (1) and (2) above. In Figure 5, we show a plot of the observed ambient magnetic field (solid brown curve) as a function of distance from the equator, h. For the purposes of calculation, we define h as the distance of the spacecraft (at nearly constant $L \sim 5.8$) from the kronographic equator (positive to the north and negative to the south). The cyclotron frequency at the location of the model equator is observed to be $f_c = 2562.9$ Hz, with a maximum estimated error of ±50 Hz, and typically ±25 Hz. In Figure 5a are plotted three curves for three different values

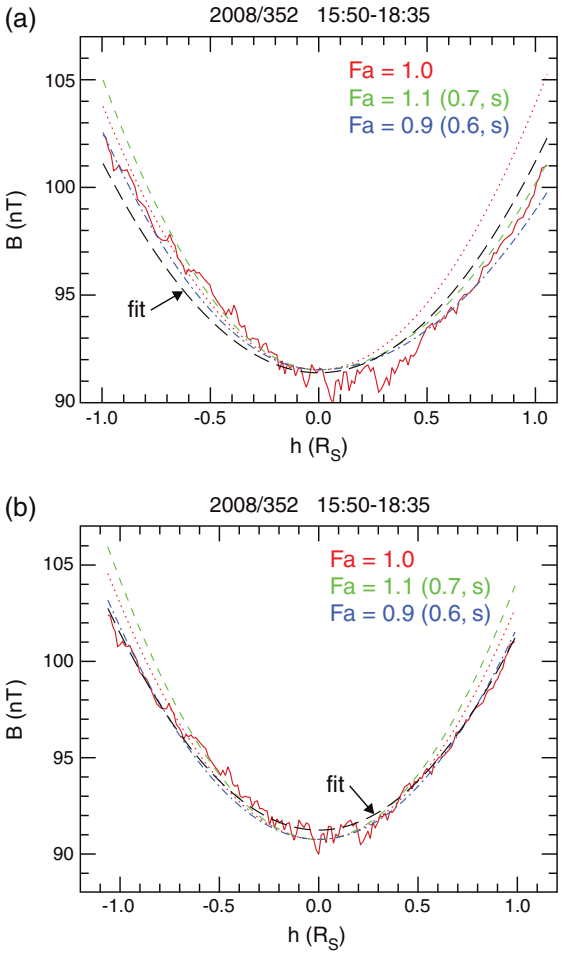

Figure 5. A plot of the observed ambient magnetic field (solid brown curve) as a function of distance from the equator, *h*. The cyclotron frequency at the equator is given the observed value, $f_c = 2562.9$ Hz. (a) Three curves plotted for three different values of $F_a = 1$ (red), 1.1(N)/0.7(S) (green), 0.9(N)/0.6(S) (blue). N (S) refers to northern (southern) hemisphere. The black, dashed curve is a least squares fit of the data to the functional form of equation (1). The least squares fitting parameters are $F_a = 0.7946$, $f_c = 2558.9$ Hz. (b) We introduce an offset of the equator by $-0.657°$ with $f_c = 2519.6$ Hz. The black, dashed curve is a least squares fit to the observed data, now with $F_a = 0.8411$.

of $F_a = 1$ (red), 1.1(N)/0.7(S) (green), 0.9(N)/0.6(S) (blue), where N (S) refers to northern (southern) hemisphere. The black, dashed curve is a least squares fit of the data to the functional form of equation (1). The least squares fitting parameters are $F_a = 0.7946$, $f_c = 2558.9$ Hz. In Figure 5b, we have introduced an offset of the equator by $-0.657°$ with $f_c = 2519.6$ Hz, corresponding to the position of the observed local minimum in the magnetic intensity. The black, dashed curve is again a least squares fit to the observed data, now with $F_a = 0.8411$. Clearly, these results indicate that a small value of F_a best fits the data. In the simulations of *Katoh and Omura* [2007, 2011] for terrestrial nonlinear chorus emissions, the authors used values of F_a ranging from 2 to 12.25, for instance. *Katoh and Omura* [2013] find that smaller values of F_a are consistent with broadband, hiss-like emission in appearance at distance from the equator with rising tones in the region close to the magnetic equator. The observed emission of 2008/352 is broadband, but it is composed of discrete, nonlinear, drifting-frequency emission only away from the equator, as reported in *Menietti et al.* [2013a]. What is observed, however, are hiss-like or diffuse emissions and an absence of drifting tones nearest the equator. This does not seem to fit the scenarios of *Katoh and Omura* [2013], which all show drifting-frequency emission everywhere, but for lower inhomogeneities, the emission becomes broadbanded and the drifting tones are washed out due to the intensity and saturation of the emission [*Katoh and Omura*, 2013, Figure 3]. Thus, while we confirm a low inhomogeneity at Saturn, the lack of drifting-frequency nonlinear structures near the equator may not be perfectly consistent with the model results presented in *Katoh and Omura* [2013], who considered field-aligned chorus only.

High-resolution data from the RPWS wideband receiver (WBR) are necessary to observe the chorus fine structure and drifting-frequency signatures. These data are available only for the electric antenna and only for specific times during equator crossings within the chorus source region. In Figure 6, we present WBR observations of drifting-frequency chorus emission observed a few degrees away from the equator. These signatures are not observed nearest to the equator where typically weaker and more diffuse (hiss-like) emission is seen. The examples come from the passes of Figures 1a and 1b. Unfortunately, there are no high-resolution data available for the passes of Figures 1c and 1d.

2.4. Chorus Bandwidth Versus Latitude

Because the pass of 2008/352 is the best example of constant L shell crossings of the equator, we use the data from this pass to more carefully examine the chorus frequency bandwidth as a function of latitude. We use a computer crosshair tool to digitalize a large sampling of points along the upper and lower edges of the chorus emission band observed in Figure 1. We limit the spectral density to values greater than 10^{-8} nT^2/Hz.

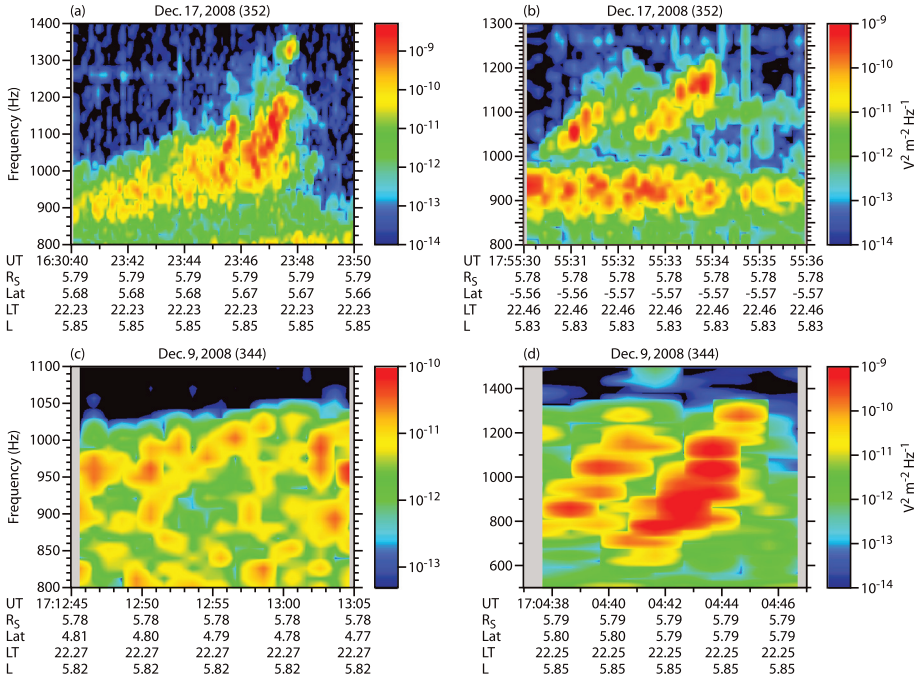

Figure 6. WBR observations of drifting-frequency chorus emission observed a few degrees away from the equator. The examples come from the passes 2008/352 and 344.

In Figure 7 we show these data along with least squares fits (dotted lines) to f_{max} and f_{min} separately. From the fits the bandwidth of the chorus is also measured (dash-dotted). We point out that the data appear to be distinguished by three different regions in each hemisphere. Starting at the equator, f_{max} increases rapidly for about 2°(near equator region), then reaches an approximate maximum (saturation) where the rate of increase becomes much smaller. This region extends for about 4°–5° (nonlinear region). It is in this region where nonlinear frequency-drifting chorus is observed [cf. *Menietti et al.,* 2013a, 2013b]. At higher latitudes, f_{max} decreases steadily (north or south region). The value of f_{min} has a much slower rate of change and appears to be reasonably fit by a single slope in each hemisphere. The functional form for the fits to the data is a simple exponential, log10 $(f) = m\lambda + b$, where f is in Hz and λ is in degrees. We list the value of m and b for each of the six regions for f_{max} and the two regions of f_{min} in Table 2.

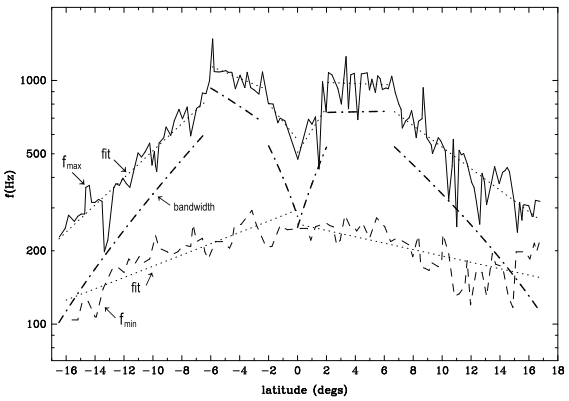

Figure 7. Plots of f_{max} and f_{min} versus latitude with least squares fits shown as dotted lines. From the fits, the bandwidth of the chorus is measured (dash-dotted). The data indicate three different regions in each hemisphere. Near the equator, f_{max} increases rapidly for about 2°, then reaches an approximate maximum where the rate of increase becomes much smaller for about 4°–5° (nonlinear region). At higher latitudes, f_{max} decreases steadily.

3. Summary and Conclusions

To study latitudinal propagation effects, we have singled out several higher inclination orbits of the Cassini spacecraft that intercept the equator near the chorus source region. Unfortunately, there are very few such passes that lie nearly along a constant L shell and nearly constant azimuth. The best example is the pass of 2008/352, Figure 1a, which provides an exemplary case for study. Other chosen data sets have provided interesting results which are similar to those seen more clearly on day 352.

Characteristic of each of the passes studied is the encounter of the most intense chorus emission

Table 2. Fit Parameters (f_{max} and f_{min})

Region	Slope (m)	Intercept (b)	Frequency
South near equator	-7.42×10^{-2}	2.76	f_{max}
South nonlinear	-2.47×10^{-2}	2.91	f_{max}
South	5.56×10^{-2}	3.27	f_{max}
North near equator	9.21×10^{-2}	2.70	f_{max}
North nonlinear	-2.21×10^{-3}	3.00	f_{max}
North	-4.41×10^{-2}	3.17	f_{max}
South	2.31×10^{-2}	2.47	f_{min}
North	-1.31×10^{-2}	2.41	f_{min}

near $L \sim 6$ at latitudes a few degrees on either side of the equator with a minimum of intensity and bandwidth nearest the equator as seen in Figure 1. The frequency range of chorus observed nearest the equator is typically $f < 1$ kHz. As $|\lambda|$ increases, the bandwidth initially increases before decreasing with latitude. Figure 1d is somewhat anomalous due to the change of local time for this pass as discussed earlier. Those orbits which intercept the chorus source regions at smaller orbit inclination (Figures 1c and 1d) observe a smaller bandwidth and intensity compared with Figures 1a and 1b. The calculated spatial growth of the chorus emission, assuming a simple exponential growth, plotted in Figure 2, shows similar characteristics, with growth away from the equator, reaching a peak, then decreasing with latitude. Variations in magnitudes can be attributed to different plasma conditions near the source regions. Not only is the spacecraft encountering different spatial regions for each pass but also undoubtedly different plasma distributions. Temporal variations are also expected but not accounted for in Figure 2.

Data from the five-channel (three magnetic and two electric) Waveform Receiver (WFR) allow analysis of chorus wave propagation characteristics, as presented in Figure 3. It is clear that the chorus emissions propagate dominantly away from the equator within 20° to 30° of the magnetic field for each of the days studied. The distribution of wave normal angle with latitude is most clearly shown in the data for day 2008/352 in Figure 4a. When the spacecraft encounters the L shell of the chorus source region, most of the chorus emission is observed within 20–30° of the magnetic field direction. The scatter at larger wave normal angles decreases with latitude. We expect a scatter of wave normal angles nearest the equator where we encounter emission coming from all directions close to the source region. Away from the source, we observe most emission propagating away from the equator. For the pass of Figure 1b (2008/344), we observe a more bursty chorus, with most emission at positive latitudes. Figure 4b shows results of wave normal angle distribution similar to Figure 4a, but with many fewer values grouped within 30° of the magnetic field. This is probably due to the more bursty nature of the chorus for the data of Figure 4b and the fact that the WFR operates in a "snapshot" mode approximately every 5 min. The WFR did not sample in phase with the bursty chorus.

Results for the passes of Figures 1c and 1d are displayed in Figures 4c and 4d, respectively. Both of these latter orbits occur along slowly changing L shells and span a range of local times as they traverse the equator compared Figures 4a and 4b; hence, we expect chorus emission from multiple sources. In Figure 4c, we see a moderate grouping of wave normal angles within 30° of magnetic field alignment when the spacecraft is closest to the L shell of strongest chorus emission. There is also a large amount of scatter of wave normal angles that may be due to multiple source regions. Unfortunately, there are no data nearest the equator for 2013/111–112. Figure 4d results are similar to Figure 4c, but a smaller concentration of wave normal angles nearest the source L shell of the chorus source region, consistent with the smaller inclination of the Cassini orbit relative to data from Figure 4a. In Figures 4c and 4d, we do not observe a slowly varying wave normal angle with latitude but rather small wave normal angles nearest the active L shell, and broad scatter elsewhere, because the source field line is encountered only briefly.

The value of magnetic field inhomogeneity for Saturn is less than that at Earth, as expected, due to the large dimensions of Saturn. This value is important to the nonlinear theory of chorus wave growth as presented by *Omura et al.* [2009] and *Katoh and Omura* [2013]. It is not clear, based on the Cassini RPWS data, if the lower inhomogeneity produces a more hiss-like (diffuse) chorus emission, as the results of *Katoh and Omura* [2013] show. The hiss-like or nonlinear broadband emission reported by *Katoh and Omura* [2013] appears diffuse on simulated spectrograms because it is saturated. The observations at Saturn do not reveal drifting chorus emission nearest the equator. This may be due to the resolution of the observations, or it may be due to linear growth nearest the equator. The nonlinear drifting-frequency emissions are observed a few degrees away from the equator.

The maximum and minimum frequencies of the chorus emission observed for 2008/352 (the clearest example studied) can be fit to a simple exponential function. An interesting observation is that f_{max} appears to be fit in

three distinct regions in each hemisphere, with a region of increasing frequency and decreasing frequency (with latitude) separated by a region of distinct nonlinear growth with f_{max} approximately constant due to the saturation of nonlinear wave growth. This pattern is not obvious at Earth and may appear at Saturn due to the much larger scale of the chorus generation region. It appears that spatial growth of chorus from sources at the equator lead to threshold-stimulated nonlinear growth a few degrees away from the equator. This transition region may be explained by parameter spaces for linear and nonlinear chorus growth as discussed by *Summers et al.* [2013]. Further investigation of details of this process are needed.

The initial estimates showed that the magnetosphere of Saturn has a rather high ratio of plasma to cyclotron frequency [*Shprits et al.*, 2012], which ensures that scattering is rather low. However, the diffusion in pitch angle and energy strongly depends on the initial spectrum as energy and pitch angle diffusion depends on the strength of the gradient in the particle distribution [*Shprits et al.*, 2012]. The latitudinal distribution of the waves, frequency distribution, and distribution of wave normal angles that is studied in this manuscript will be crucial for modeling the competition of acceleration and loss with 2-D codes [*Horne et al.*, 2008; *Shprits et al.,* 2012; *Woodfield et al.,* 2013] and future 3-D codes solving for the evolution of electron phase space density at Saturn in terms of the radial distance, pitch angle, and energy.

Acknowledgments

We wish to thank J. Barnholdt for administrative assistance, J. Chrisinger for help with several figures, and T. Averkamp for assistance with the WNA code. J.D.M. acknowledges support from JPL contract 1415150 and NASA grant NNX11AM36G. Cassini RPWS data are archived in calibrated, full resolution at the NASA Planetary Data System website: http://pds.nasa.gov/ds-view/pds/viewDataset.jsp?dsid=CO-V/E/J/S/SS-RPWS-3-RDR-LRFULL-V1.0. The calibrated, full resolution WFR data are located at the same site: dsid = CO-V/E/J/S/SS-RPWS-2-REFDR-WFRFULL-V1.0.

Michael Balikhin thanks Ondrej Santolik and an anonymous reviewer for their assistance in evaluating this paper.

References

Gurnett, D. A., et al. (2004), The Cassini radio and plasma wave investigation, *Space Sci. Rev.*, *114*, 395–463, doi:10.1007/s11214-004-1434-0.

Haque, N., U. S. Inan, T. F. Bell, and J. S. Pickett (2012), Spatial dependence of banded chorus intensity near the magnetic equator, *Geophys. Res. Lett.*, *39*, L17103, doi:10.1029/2012GL052929.

Hill, T. W., A. M. Rymer, J. L. Burch, F. J. Crary, D. T. Young, M. F. Thomsen, D. Delapp, N. Andre, A. J. Coates, and G. R. Lewis (2005), Evidence of rotationally driven plasma transport in Saturn's magnetosphere, *Geophys. Res. Lett.*, *32*, L14S10, doi:10.1029/2005GL022620.

Horne, R. B., S. A. Glauert, and R. M. Thorne (2003), Resonant diffusion of radiation belt electrons by whistler-mode chorus, *Geophys. Res. Lett.*, *30*(9), 1493, doi:10.1029/2003GL016963.

Horne, R. B., R. M. Thorne, S. A. Glauert, J. D. Menietti, Y. Y. Shprits, and D. A. Gurnett (2008), Gyro-resonant electron acceleration at Jupiter, *Nat. Phys.*, *4*, 301–304, doi:10.1038/nphys897.

Hospodarsky, G. B., T. F. Averkamp, W. S. Kurth, D. A. Gurnett, J. D. Menietti, O. Santolik, and M. K. Dougherty (2008), Observations of chorus at Saturn using the Cassini Radio and Plasma Wave Science instrument, *J. Geophys. Res.*, *113*, A12206, doi:10.1029/2008JA013237.

Hospodarsky, G. B., K. Sigsbee, J. S. Leisner, J. D. Menietti, W. S. Kurth, D. A. Gurnett, C. A. Kletzing, and O. Santolik (2012), Plasma wave observations at Earth, Jupiter, and Saturn, in *Dynamics of the Earth's Radiation Belts and Inner Magnetosphere*, *Geophys. Monogr. Ser.*, vol. 199, edited by D. Summers et al., pp. 415–430, AGU, Washington, D. C.

Katoh, Y., and Y. Omura (2007), Computer simulation of chorus wave generation in the Earth's inner magnetosphere, *Geophys. Res. Lett.*, *34*, L03102, doi:10.1029/2006GL028594.

Katoh, Y., and Y. Omura (2011), Amplitude dependence of frequency sweep rates of whistler mode chorus emissions, *J. Geophys. Res.*, *116*, A07201, doi:10.1029/2011JA016496.

Katoh, Y., and Y. Omura (2013), Effect of the background magnetic field inhomogeneity on generation processes of whistler-mode chorus and broadband hiss-like emissions, *J. Geophys. Res. Space Physics*, *118*, 4189–4198, doi:10.1002/jgra.50395.

LeDocq, M. J., D. A. Gurnett, and G. B. Hospodarsky (1998), Chorus source location from VLF Poynting flux measurements with the Polar spacecraft, *Geophys. Res. Lett.*, *25*, 4063–4066, doi:10.1029/1998GL900071.

Li, W., Y. Y. Shprits, and R. M. Thorne (2007), Dynamic evolution of energetic outer zone electrons due to wave-particle interactions during storms, *J. Geophys. Res.*, *112*, A10220, doi:10.1029/2007JA012368.

Li, W. B., R. M. Thorne, J. Bortnik, J. C. Green, C. A. Kletzing, C. A. Kletzing, W. S. Kurth, and G. B. Hospodarsky (2013), Constructing the global distribution of chorus wave intensity using measurements of electrons by the POES satellites and waves by the Van Allen Probes, *Geophys. Res. Lett.*, *40*, 4526–4532, doi:10.1002/grl.50920.

Mauk, B. H., and N. J. Fox (2010), Electron radiation belts of the solar system, *J. Geophys. Res.*, *115*, A12220, doi:10.1029/2010JA015660.

Means, J. D. (1972), Use of the three-dimensional covariance matrix in analyzing the polarization properties of plane waves, *J. Geophys. Res.*, *77*, 5551–5559, doi:10.1029/JA077i028p05551.

Menietti, J. D., O. Santolik, A. M. Rymer, G. B. Hospodarsky, A. M. Persoon, D. A. Gurnett, A. J. Coates, and D. T. Young (2008), Analysis of plasma waves observed within local plasma injections seen in Saturn's magnetosphere, *J. Geophys. Res.*, *113*, A05213, doi:10.1029/2007JA012856.

Menietti, J. D., Y. Y. Shprits, R. B. Horne, E. E. Woodfield, G. B. Hospodarsky, and D. A. Gurnett (2012), Chorus, ECH, and Z mode emissions observed at Jupiter and Saturn and possible electron acceleration, *J. Geophys. Res.*, *117*, A12214, doi:10.1029/2012JA018187.

Menietti, J. D., Y. Katoh, G. B. Hospodarsky, and D. A. Gurnett (2013a), Frequency drift of Saturn chorus emission compared to nonlinear theory, *J. Geophys. Res. Space Physics*, *118*, 982–990, doi:10.1002/jgra.50165.

Menietti, J. D., P. Schippers, Y. Katoh, J. S. Leisner, G. B. Hospodarsky, D. A. Gurnett, and O. Santolik (2013b), Saturn chorus intensity variations, *J. Geophys. Res. Space Physics*, *118*, 5592–5602, doi:10.1002/jgra.50529.

Omura, Y., N. Furuya, and D. Summers (2007), Relativistic turning acceleration of resonant electrons by coherent whistler mode waves in a dipole magnetic field, *J. Geophys. Res.*, *112*, A06236, doi:10.1029/2006JA012243.

Omura, Y., Y. Kato, and D. Summers (2008), Theory and simulation of the generation of whistler-mode chorus, *J. Geophys. Res.*, *113*, A04223, doi:10.1029/2007JA012622.

Omura, Y., M. Hikishima, Y. Katoh, D. Summers, and S. Yagitani (2009), Nonlinear mechanisms of lower-band and upper-band VLF chorus emissions in the magnetosphere, *J. Geophys. Res.*, *114*, A07217, doi:10.1029/2009JA014206.

Santolik, O. (2008), New results of investigations of whistler-mode chorus emissions, *Nonlinear Process. Geophys.*, *15*, 621–630, doi:10.5194/npg-15-621-2008.

Santolík, O., D. A. Gurnett, J. S. Pickett, J. Chum, and N. Cornilleau-Wehrlin (2009), Oblique propagation of whistler mode waves in the chorus source region, *J. Geophys. Res.*, *114*, A00F03, doi:10.1029/2009JA014586.

Shprits, Y. Y., and B. Ni (2009), Dependence of the quasi-linear scattering rates on the wave normal distribution of chorus waves, *J. Geophys. Res. 114*, A11205, doi:10.1029/2009JA014223.

Shprits, Y. Y., R. M. Thorne, R. B. Horne, and D. Summers (2006), Bounce-averaged diffusion coefficients for field-aligned chorus waves, *J. Geophys. Res.*, *111*, A10225, doi:10.1029/2006JA011725.

Shprits, Y. Y., N. P. Meredith, and R. M. Thorne (2007), Parameterization of radiation belt electron loss timescales due to interactions with chorus waves, *Geophys. Res. Lett.*, *34*, L11110, doi:10.1029/2006GL029050.

Shprits, Y. Y., J. D. Menietti, X. Gu, K. C. Kim, and R. B. Horne (2012), Gyroresonant interactions between the radiation belt electrons and whistler mode chorus waves in the radiation environments of Earth, Jupiter, and Saturn: A comparative study, *J. Geophys. Res.*, *117*, A11216, doi:10.1029/2012JA018031.

Spasojevic, M., and Y. Y. Shprits (2013), Chorus functional dependencies derived from CRRES data, *Geophys. Res. Lett.*, *40*, 3793–3797, doi:10.1002/grl.50755.

Summers, D., Y. Omura, Y. Miyashita, and D.-H. Lee (2012), Nonlinear spatiotemporal evolution of whistler mode chorus waves in Earth's inner magnetosphere, *J. Geophys. Res.*, *117*, A09206, doi:10.1029/2012JA017842.

Summers, D., R. Tang, Y. Omura, and D.-H. Lee (2013), Parameter spaces for linear and nonlinear whistler-mode waves, *Phys. Plasmas*, *20*, 072110, doi:10.1063/1.4816022.

Tang, R., and D. Summers (2012), Energetic electron fluxes at Saturn from Cassini observations, *J. Geophys. Res.*, *117*, A06221, doi:10.1029/2011JA017394.

Thorne, R. M., T. P. O'Brien, Y. Y. Shprits, D. Summers, and R. B. Horne (2005), Timescale for MeV electron microburst loss during geomagnetic storms, *J. Geophys. Res.*, *110*, A09202, doi:10.1029/2004JA010882.

Trakhtengerts, V. Y., A. G. Demekhov, E. E. Titova, B. V. Kozelov, O. Santolik, D. Gurnett, and M. Parrot (2004), Interpretation of Cluster data on chorus emissions using the backward wave oscillator model, *Phys. Plasmas*, *11*, 1345–1351, doi:10.1063/1.1667495.

Woodfield, E. E., R. B. Horne, S. A. Glauert, J. D. Menietti, and Y. Y. Shprits (2013), Electron acceleration at Jupiter: Input from cyclotron-resonant interaction with whistler-mode chorus waves, *Ann. Geophys.*, *31*, 1619–1630, doi:10.5194/angeo-31-1619-2013.